Molecular Characteristics of Repotrectinib That Enable Potent Inhibition of TRK Fusion Proteins and Resistant Mutations

Brion W. Murray[1], Evan Rogers[1], Dayong Zhai[1], Wei Deng[1], Xi Chen[2], Paul A. Sprengeler[1], Xin Zhang[1], Armin Graber[1], Siegfried H. Reich[1], Shanna Stopatschinskaja[1], Benjamin Solomon[3], Benjamin Besse[4], and Alexander Drilon[5]

ABSTRACT

NTRK chromosomal rearrangements yield oncogenic TRK fusion proteins that are sensitive to TRK inhibitors (larotrectinib and entrectinib) but often mutate, limiting the durability of response for $NTRK^+$ patients. Next-generation inhibitors with compact macrocyclic structures (repotrectinib and selitrectinib) were designed to avoid resistance mutations. Head-to-head potency comparisons of TRK inhibitors and molecular characterization of binding interactions are incomplete, obscuring a detailed understanding of how molecular characteristics translate to potency. Larotrectinib, entrectinib, selitrectinib, and repotrectinib were characterized using cellular models of wild-type TRKA/B/C fusions and resistance mutant variants with a subset evaluated in xenograft tumor models. Crystal structures were determined for repotrectinib bound to TRKA (wild-type, solvent-front mutant). TKI-naïve and pretreated case studies are presented. Repotrectinib was the most potent inhibitor of wild-type TRKA/B/C fusions and was more potent than selitrectinib against all tested resistance mutations, underscoring the importance of distinct features of the macrocycle structures. Cocrystal structures of repotrectinib with wild-type TRKA and the $TRKA^{G595R}$ SFM variant elucidated how differences in macrocyclic inhibitor structure, binding orientation, and conformational flexibility affect potency and mutant selectivity. The SFM crystal structure revealed an unexpected intramolecular arginine sidechain interaction. Repotrectinib caused tumor regression in *LMNA–NTRK1* xenograft models harboring GKM, SFM, xDFG, and GKM + SFM compound mutations. Durable responses were observed in TKI-naïve and -pretreated patients with $NTRK^+$ cancers treated with repotrectinib (NCT03093116). This comprehensive analysis of first- and second-generation TRK inhibitors informs the clinical utility, structural determinants of inhibitor potency, and design of new generations of macrocyclic inhibitors.

Introduction

Chromosomal rearrangement of neurotrophin receptor tyrosine kinase genes (*NTRK1*, *NTRK2*, and *NTRK3*) encoding tropomyosin receptor tyrosine kinases (TRKA, TRKB, and TRKC) create oncogenic fusion proteins in a range of cancers (1–3). Patients harboring these gene fusions have high response rates to treatment with the first-generation TRK tyrosine kinase inhibitors (TKI) larotrectinib and entrectinib (**Fig. 1A**; ref. 4). Larotrectinib received FDA approval for treatment of patients with solid tumors harboring *NTRK* gene fusions and has a 79% overall response rate, a 35.2-month median duration of response, and a 16% complete response rate in a pooled analysis of 159 patients with solid tumors (5). Clinical studies of entrectinib report a 57% overall response rate, 10.4-month median duration of response, and 7% complete response rate in 54 patients with $NTRK^+$ solid tumors (6). The effectiveness of these agents is often limited by the emergence of drug resistance (3, 4) from mutations in distinct regions of the active site of the TRK kinase domain (solvent-front region, SFM; gatekeeper residue, GKM; activation loop, xDFG; refs. 1, 4, 7–10; **Fig. 1B**). In addition, the emergence of compound mutations (multiple mutations in an active site) is possible based on clinical experience with therapies targeting related *ABL*, *ALK*, *RET*, and *ROS1* fusion protein-dependent cancers (11–13). Taken together, there are a range of clinically relevant TRKA/B/C resistance mutations that abrogate the clinical responses to first-generation TRK inhibitors, and the landscape of resistance mutations is expected to expand.

The second-generation TRK inhibitors repotrectinib (TPX-0005; ref. 14) and selitrectinib (LOXO-195; ref. 9) have compact macrocyclic structures (**Fig. 1A**) that were designed to limit adverse interactions with resistance mutation hotspots because of their small binding interface. However, subtle differences in macrocycle structure can significantly affect inhibitor potency and predicting binding interactions via molecular modeling has limitations (15). Preclinical and clinical studies of repotrectinib show that it is effective against mutations in the solvent-front region (e.g., $ETV6–NTRK3^{G623E}$) that arise during treatment with first-generation inhibitors (14). Selitrectinib has reported efficacy against mutations in the solvent-front and xDFG regions (9). To date, however, there are no direct comparisons of the compact macrocyclic TRK inhibitors, limiting our understanding of how elements of inhibitor structure contribute to preclinical potency and clinical efficacy. A detailed understanding of macrocyclic inhibitor interactions with TRK fusion proteins and molecular mechanisms of resistance mutations is therefore needed.

[1]Turning Point Therapeutics, San Diego, California. [2]Wuxi Biortus Biosciences Co., Ltd., Jiangyin, Jiangsu, China. [3]Peter MacCallum Cancer Center, Melbourne, Australia. [4]CLCC Institut Gustave Roussy, Villejuif Cedex, France. [5]Memorial Sloan Kettering Cancer Center, Weill Cornell Medical College, New York, New York.

Note: Supplementary data for this article are available at Molecular Cancer Therapeutics Online (http://mct.aacrjournals.org/).

Corresponding Author: Brion W. Murray, Turning Point Therapeutics, 10628 Science Center Drive, Suite 200, San Diego, CA 92121. Phone: 858-926-5251; E-mail: brion.murray@tptherapeutics.com

Mol Cancer Ther 2021;20:2446–56

doi: 10.1158/1535-7163.MCT-21-0632

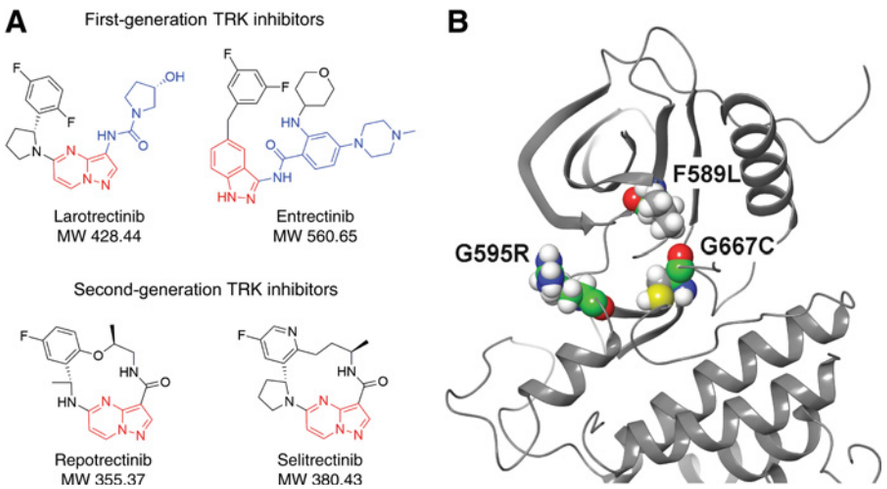

Figure 1.
TRK inhibitor molecular structures and TRKA resistance mutation locations. **A,** Structures and sizes of first- and second-generation inhibitors of TRK. The red coloring in the structure denotes the hinge-binding moiety, and the blue color identifies the motif that extends into the solvent-front region. **B,** TRKA positions of the solvent-front (e.g., TRKA^{G595R}), gatekeeper (e.g., TRKA^{F589L}), and activation loop xDFG (e.g., TRKA^{G667C}) mutations.

In this study, the first- and second-generation TRK inhibitors were profiled against TRKA/B/C and their resistance mutations in cellular models, with follow-up analyses in *in vivo* xenograft tumor models. Crystallographic characterization of molecular interactions of the compact macrocyclic inhibitor repotrectinib with wild-type TRKA and TRKA harboring a G595R SFM was undertaken. We also performed a similar molecular characterization of the binding of the macrocyclic inhibitor selitrectinib using the TRKA cocrystal structures to more accurately model molecular interactions. Finally, we present case studies of patients with TKI-naïve and TKI-pretreated *NTRK*$^+$ cancers who were treated with repotrectinib, demonstrating clinical translation of the preclinical findings.

Materials and Methods

Reagents and chemicals

Larotrectinib and selitrectinib were purchased from MedChemExpress; entrectinib was purchased from Medkoo Bioscience. Repotrectinib was provided by Turning Point Therapeutics.

Cloning, expression, and purification of the kinase domain of TRKA

NIH3T3 and Ba/F3 cell lines were purchased from DSMZ. The KM12 cell line was obtained from the NCI Division of Cancer Treatment and Diagnosis tumor cell repository. Cell lines were confirmed to be *mycoplasma*-free (Biomiga) and were used between 3 and 10 passages. The human TRKA kinase domain (amino acid residues 502–796) with an N-terminal 6x-His tag and TEV cleavage site was synthesized, inserted into the pFastbacHTB vector (Life Technologies) for baculovirus protein expression, and used to generate recombinant baculovirus using the Bac-to-Bac system (Life Technologies) following the manufacturer's protocol. SF21 cells were infected at 2.0 $\times$ 10^6/mL. The pFastbacHTB for TRKA^{G595R} mutant was made by site-directed mutagenesis. The relative upstream and downstream primers were designed by Sangon Bioengineering Co. Recombinant baculovirus of TRKA^{G595R} was generated in a similar manner to wild-type TRKA.

Cells were harvested 48 hours after infection by centrifugation (5 minutes, 9,000 rpm, 4°C), lysed in a high-pressure homogenizer, pelleted by centrifugation, supernatant collected, purified by Ni-NTA–agarose in a Econo-Pac column (Bio-Rad): two wash steps (50 mmol/L Tris-HCl pH 8.0, 500 mmol/L NaCl, 5% glycerol; 10 mmol/L imidazole high-salt buffer) and eluted with 300 mmol/L imidazole high-salt buffer. The histidine affinity tag was removed by overnight TEV protease incubation, His-trap FF column, and a 16/60 Superdex 200 gel filtration with 20 mmol/L Tris-HCl (pH 8.0) and 100 mmol/L NaCl, and 2 mmol/L dithiothreitol (DTT). TRKA eluted in a symmetric peak at the expected size, concentrated to 10.3 mg/mL, and stored at −80°C. Electrospray mass spectrometry revealed a major peak at the expected TRKA kinase domain mass with 95% purity. The purification strategy for TRKA^{G595R} was similar with further purification using ion exchange chromatography (Mono Q 5/50, GE Healthcare) and gel filtration (Hiload 16/60 Superdex 200 size exclusion column, GE Healthcare) in a buffer containing 20 mmol/L Tris-HCl (pH 8.0), 100 mmol/L NaCl, and 2 mmol/L DTT. The protein was concentrated to 3.92 mg/mL and stored at −80°C.

Crystallization and data collection

The sitting drop vapor diffusion method was used to obtain the initial crystal of TRKA after two days at 293 K in 8 mol/L ammonium sulfate, 0.1 mol/L citric acid, pH 5.0. TRKA^{G595R} crystals appeared after four days in 3.0 mol/L NaCl, 0.1 mol/L Bis-Tris pH 6.5 as mother liquor. Crystals of TRKA and TRKA^{G595R} were soaked with 0.5 mmol/L repotrectinib for 2 hours before being transferred to the mother liquor with the addition of 25% glycerol as cryoprotectant.

Crystals were screened using a Rigaku diffraction system (Applied Rigaku Technologies, Inc.), and high-quality crystals of the TRKA–repotrectinib complex, TRKA^{G595R}, and the TRKA^{G595R}–repotrectinib complex were flash frozen in liquid nitrogen. Diffraction data were collected at a wavelength of 0.9792 Å using a Dectris Eiger 16 M detector in beamline BL17U (Shanghai Synchrotron Radiation Facility). Data were processed using the HKL2000 package (HKL Research Inc.).

The structure of unbound repotrectinib was determined by single-crystal X-ray diffraction using Cu K-alpha radiation with analysis of the intensity and phase shifting caused by anomalous dispersion. Measurements were made using a Nonius FR-591 rotating-anode source and fine-focus optics in conjunction with a Bruker APEX-II diffractometer (Bruker Corporation).

Structure determination

Structure determination was done using the CCP4 suite of programs (CCP4) and solved by molecular replacement with PHASER-MR (PDB 4YNE as a starting model). REFMAC5 and Coot were used for further iterative refinement and manual model rebuilding. Molecular

figures were prepared using PyMOL (Schrödinger, Inc.). Details of data collection and structure determination are summarized in Supplementary Table S1. TRK cocrystal structure coordinates have been deposited in the PDB (7VKO, 7VKM, and 7VKN).

Molecular modeling

Inhibitor docking simulations used Glide software (Schrödinger) in Standard Precision mode. Possible conformers of repotrectinib and selitrectinib were generated using Schrödinger's Prime Macrocycle Sampling process (Schrödinger Inc) sampling 1,000 conformations for each molecule; 17 conformations of repotrectinib and 18 conformations of selitrectinib were generated. DFT *Ab initio* analysis with Jaguar software (Schrödinger Inc.) using B3LYP-D3 theory, and the 6-31G** basis set with geometry optimization was used to predict low-energy conformers of repotrectinib and selitrectinib.

Cancer cell culture and preparation

NIH3T3 and KM12 cells were cultured using standard techniques in DMEM (Corning, Inc.) with 10% fetal bovine serum (Thermo Fisher Scientific, Inc) and 100 U/mL of penicillin/streptomycin (Corning, Inc.) at 37°C in a humidified atmosphere with 5% CO_2. Ba/F3 cells were cultured using standard techniques in RPMI-1640 medium (Corning, Inc.) with 10% fetal bovine serum (Thermo Fisher Scientific, Inc.) at 37°C in a humidified atmosphere with 5% CO_2.

Stable cell lines

To generate the engineered cell lines, the *LMNA–NTRK1*, *TEL–NTRK2*, *TEL–NTRK3* fusion genes and fusion genes with the corresponding mutation were synthesized at GenScript and cloned into pCDH-CMV-MCS-EF1-Puro plasmid (System Biosciences, Inc). Ba/F3 or NIH3T3 cells were infected with lentivirus containing the wild-type or mutant genes. The engineered NIH3T3 cells were selected in DMEM supplemented with 10% fetal bovine serum, 100 U/mL of penicillin, and 1 μg/mL puromycin solution. The engineered Ba/F3 cell lines were selected in RPMI-1640 supplemented with 10% fetal bovine serum, 100 U/mL penicillin, 10 ng/mL IL3 (Life Technologies), and 1 μg/mL puromycin solution followed by a further selection in the same medium without IL3.

Evaluation of cell proliferation and kinase phosphorylation

KM12 cells harboring the *TPM3–NTRK1* fusion gene and stable Ba/F3 or NIH3T3 cells transduced with *NTRK1, 2*, and *3* fusion genes (wild-type or mutants) were cultured using standard techniques in DMEM or RPMI-1640 medium with 10% fetal bovine serum, 100 U/mL of penicillin/streptomycin (Corning, Inc.) at 37°C in 5% CO_2. For cell proliferation assays, 2,000 KM12 cells or transduced Ba/F3 cells per well were seeded in 384-well white plate and then treated for 72 hours. Cell proliferation was measured using CellTiter-Glo luciferase-based ATP detection assay (Promega) following the manufacturer's protocol. IC_{50} values were determined using Prism software (GraphPad Software). For immunoblotting of cellular phosphorylation assays, half a million KM12 or engineered NIH3T3 cells harboring mutant LMNA–TRKA per well were seeded in 24-well plate for 24 hours prior to treatment. Cells were collected after a 4-hour treatment and lysed in RIPA buffer. Protein lysates were resolved on 4%–12% Bolt Bis-Tris gels with MES running buffer, transferred to nitrocellulose membrane using Trans-Blot Turbo Transfer System (Bio-Rad), and detected with desired antibodies. Antibodies were incubated overnight at 4°C, washed, incubated with corresponding HRP-conjugated secondary antibodies, and incubated with chemiluminescent substrate for 5 minutes at room temperature. Chemiluminescent images were acquired with a C-DiGit Imaging System (LI-COR Biosciences). The relative density of the chemiluminescent bands was quantified via Image Studio Digits from LI-COR (LI-COR Biosciences).

Evaluation of repotrectinib in subcutaneous xenograft NIH3T3 LMNA–TRKA models harboring G595R, F589L, and F589L/G595R tumors in athymic nude mice

NIH3T3 cells with LMNA–TRKA fusion harboring F589L, G595R, or F589L/G595R mutations were subcutaneously inoculated in athymic nude mice. Treatment was initiated after the mean tumor volume reached about 150–250 mm^3; tumor volume and body weight were measured during treatment. Tumor growth inhibition (TGI) was calculated based on changes in tumor volume for treated (T) over control (C) group:

$$\text{TGI} = (1 - \Delta T/\Delta C) \times 100\% \text{ when } \Delta T > 0;$$
$$\text{TGI} = (2 - T_i/T_0) \times 100\% \text{ when } \Delta T < 0$$

where ΔT was the change in average tumor volume between time i and time 0 in the treated group, ΔC was the change in average tumor volume in the control group, T_i was the average tumor volume at time i and T_0 was the average tumor volume at time 0. A TGI > 100% indicated a regression in tumors. Tumor regression was calculated as $(1 - T_i/T_0) \times 100\%$.

Study design and conduct, and sample identification

Repotrectinib is being investigated in a first-in-human dose-escalation phase I and registrational phase II study (TRIDENT-1; NCT03093116). TKI-naïve and TKI-refractory patients with advanced *ROS1/TRK/ALK*$^+$ solid tumors were treated with repotrectinib at dose levels from 40 mg q.d. to 200 mg b.i.d. (16). The study was conducted in accordance with the Declaration of Helsinki, and the protocol was approved by the institutional review boards at each participating site. Written informed consent was obtained from all the patients before screening.

Blood samples were collected before treatment and at progression from patients with *NTRK* gene fusion–positive tumors who were enrolled in the phase I part of the study. Samples were tested for *NTRK* fusions using the Guardant360 assay in a CLIA-certified, College of American Pathologists (CAP)-accredited, New York State Department of Health-approved laboratory at Guardant Health in Redwood City, CA.

cfDNA isolation and next-generation sequencing

cfDNA for the Guardant360 next-generation sequencing panel was isolated at Guardant Health from plasma from patients in the phase I study as previously described (17). Briefly, up to 30 ng of cfDNA was extracted from 1 to 2 mL of plasma (QIAmp Circulating Nucleic Acid Kit, Qiagen, Inc.) and labeled with nonrandom oligonucleotide barcodes (IDT, Inc.). This was used for library preparation and enrichment by hybridization capture (Agilent Technologies), pooled, and sequenced by paired-end synthesis using a NextSeq 500 (Illumina). The resulting sequence data were analyzed on a locked, previously validated, custom bioinformatics pipeline. Separate sequencing controls were utilized for single-nucleotide variants, insertions, and deletions, copy-number alterations, and gene fusions.

Results

Cellular characterization of TRK inhibitor potency against oncogenic TRK and drug-resistance mutations

Both first-generation (larotrectinib and entrectinib) TRK inhibitors with extended molecular structures and second-generation (repotrectinib

Table 1. Potency of first- and second-generation TRK inhibitors in cell proliferation assays of Ba/F3 cells engineered with TRK fusions (*LMNA–TRKA*, *ETV6–TRKB*, and *ETV6–TRKC*). All data were derived from three independent replicates.

IC_{50} (±SD) TRK mutation			First generation		Second generation	
			Larotrectinib	Entrectinib	Selitrectinib	Repotrectinib
No mutation	TRKA	WT	23.5 ± 8.6	0.30 ± 0.10	3.9 ± 4.2	<0.2
	TRKB	WT	36.5 ± 20.8	0.80 ± 0.50	1.8 ± 0.9	<0.2
	TRKC	WT	49.4 ± 22.8	1.3 ± 1.0	3.0 ± 2.9	<0.2
Solvent front	TRKA	G595R	3,540 ± 1,560	987 ± 487	18.7 ± 6.4	0.2 ± 0.1
	TRKB	G639R	3,670 ± 2,080	1,690 ± 470	28.8 ± 16	2.6 ± 2.2
	TRKC	G623R	6,940 ± 1,090	1,500 ± 440	27.7 ± 6.8	2.0 ± 1.8
	TRKC	G623E	1,510 ± 680	1,470 ± 220	27.0 ± 20.4	0.40 ± 0.40
Gatekeeper	TRKA	F589L	675 ± 137	<0.2	27.8 ± 5.6	<0.2
	TRKB	F623L	5,730 ± 1,580	6.4 ± 3.7	85.4 ± 24.4	<0.2
	TRKC	F617I	4,330 ± 1,150	60.4 ± 11.7	51.8 ± 22.5	<0.2
xDFG	TRKA	G667C	1,630 ± 270	138 ± 82	118 ± 31	11.8 ± 7.3
	TRKB	G709C	3,450 ± 510	876 ± 309	341 ± 86	67.6 ± 22
	TRKC	G696C	4,360 ± 1,470	547 ±339	182 ± 51	19.5 ± 12.1
Compound mutation	TRKA	G595R F589L	>10,000	1,840 ± 250	468 ± 55	17.7 ± 7.8

and selitrectinib) compact macrocyclic TRK inhibitors (**Fig. 1A**) were profiled against TRKA, TRKB, and TRKC, and a range of resistance mutations, using a panel of engineered Ba/F3 cell proliferation assays performed with sufficient replicates ($n = 3$) to enable meaningful comparisons (**Table 1**). There were different degrees of potency against wild-type TRKA, TRKB, and TRKC fusions, with IC_{50} values of 23.5–49.4 nmol/L for larotrectinib, 0.3–1.3 nmol/L for entrectinib, 1.8–3.9 nmol/L for selitrectinib, and <0.2 nmol/L for repotrectinib. First-generation TRK inhibitors had reduced potency against a range of active-site mutations. Larotrectinib had reduced potency against all classes of TRK mutations (IC_{50} >600 nmol/L). Entrectinib had >400-fold decreases in potency against SFM, xDFG, and compound TRK mutations with a wide range of potencies against the GKM (IC_{50} <0.2–60.4 nmol/L). Entrectinib was highly potent against the TRKA GKM with the same potency as repotrectinib (IC_{50} < 0.2 nmol/L) but against TRKB and TRKC it was 30–300-fold less potent than repotrectinib. Macrocyclic inhibitors selitrectinib and repotrectinib potencies were less affected by resistance mutations; however, repotrectinib was approximately 10-fold more potent against SFM and compound mutations and 100-fold more potent against GKM. For TRKA/B/C xDFG mutations, larotrectinib was inactive (IC_{50} > 1500 nmol/L), modest potency was observed for both entrectinib (IC_{50} = 138–876 nmol/L) and selitrectinib (IC_{50} 124–341 nmol/L), and repotrectinib had moderate potency (IC_{50} 14.6–67.6 nmol/L). This analysis of the four TRK inhibitors against a range of TRK variants demonstrates unique patterns of potency for each inhibitor, consistent with distinct interactions with TRK and drug-resistant variants.

To confirm and extend inhibitor characterization of potency in cell proliferation assays, pharmacodynamic effects were evaluated in cells harboring wild-type and mutated forms of TRKA. Autophosphorylation of TRKA-Tyr490 was selected as a marker of TRKA activation as this creates a docking site that enables PI3K/AKT and MAPK signaling (18, 19). In KM12 tumor cells harboring a wild-type *TPM3-TRKA* fusion, inhibition of TRKA autophosphorylation and activation of downstream signaling was evaluated for all four TRK inhibitors (**Fig. 2**). Repotrectinib was the most potent inhibitor of TRKA autophosphorylation (IC_{50} < 0.03 nmol/L) and required a lower concentration range (0–30 nmol/L) than the other TRK inhibitors (0–300 nmol/L) to capture its potency (**Fig. 2A**). Inhibition of ERK phosphorylation was well correlated with inhibition of TRK autophosphorylation. All four inhibitors partially inhibited AKT phosphorylation, with potency correlating with inhibition of TRK autophosphorylation. Inhibition of TRKA-Tyr490 phosphorylation in an engineered cell line harboring *LMNA–TRKA* was consistent with the results in KM12 tumor cells (Supplementary Fig. S1). Pharmacodynamic modulation of TRK autophosphorylation was evaluated in engineered NIH3T3 LMNA–TRKA^{G595R} cells. Repotrectinib was highly potent against LMNA–TRKA^{G595R} (IC_{50} < 0.3 nmol/L), whereas first-generation TRK inhibitors had minimal activity (IC_{50} 300–1000 nmol/L; Supplementary Fig. S1).

A direct comparison of compact macrocyclic inhibitors was performed in pharmacodynamic cellular assays of TRKA harboring G595R SFM, F589 L GKM, and F589L/G595R compound mutations (**Fig. 2B**). Repotrectinib was approximately 10-fold more potent than selitrectinib against the F589 L TRKA GKM and 3- to 10-fold more potent against TRKA harboring a G595R mutation. Repotrectinib had significant potency (IC_{50} 10–30 nmol/L) against the TRKA F589L/G595R compound mutation, against which selitrectinib was less active (IC_{50} > 300 nmol/L). As TRKA pharmacodynamic cellular results were well correlated with TRKA-dependent cell proliferation potency, a similar correlation of antiproliferation potency to pharmacodynamic potency for TRKB and TRKC can be anticipated. The analysis of repotrectinib and selitrectinib illustrates that structurally related compact macrocyclic inhibitors can have substantial differences in potency.

Binding interactions of repotrectinib with the TRKA active site

Understanding potency differences between the second-generation inhibitors requires an understanding of both steric and energetic contributions. To date, neither a kinase crystal structure with a G/R SFM nor a cocrystal structure of TRK with the compact macrocyclic inhibitors has been reported. To address these gaps, a series of cocrystal structures were solved: wild-type TRKA with repotrectinib, and TRKA harboring the G595R SFM (with and without repotrectinib; **Fig. 3**; Supplementary Table S1). Repotrectinib binds in the hinge region of the wild-type TRKA ATP binding pocket (**Fig. 3A** and **B**). Complete electron density is observed for repotrectinib bound in the active site of wild-type TRKA to enable precise assignment of interactions

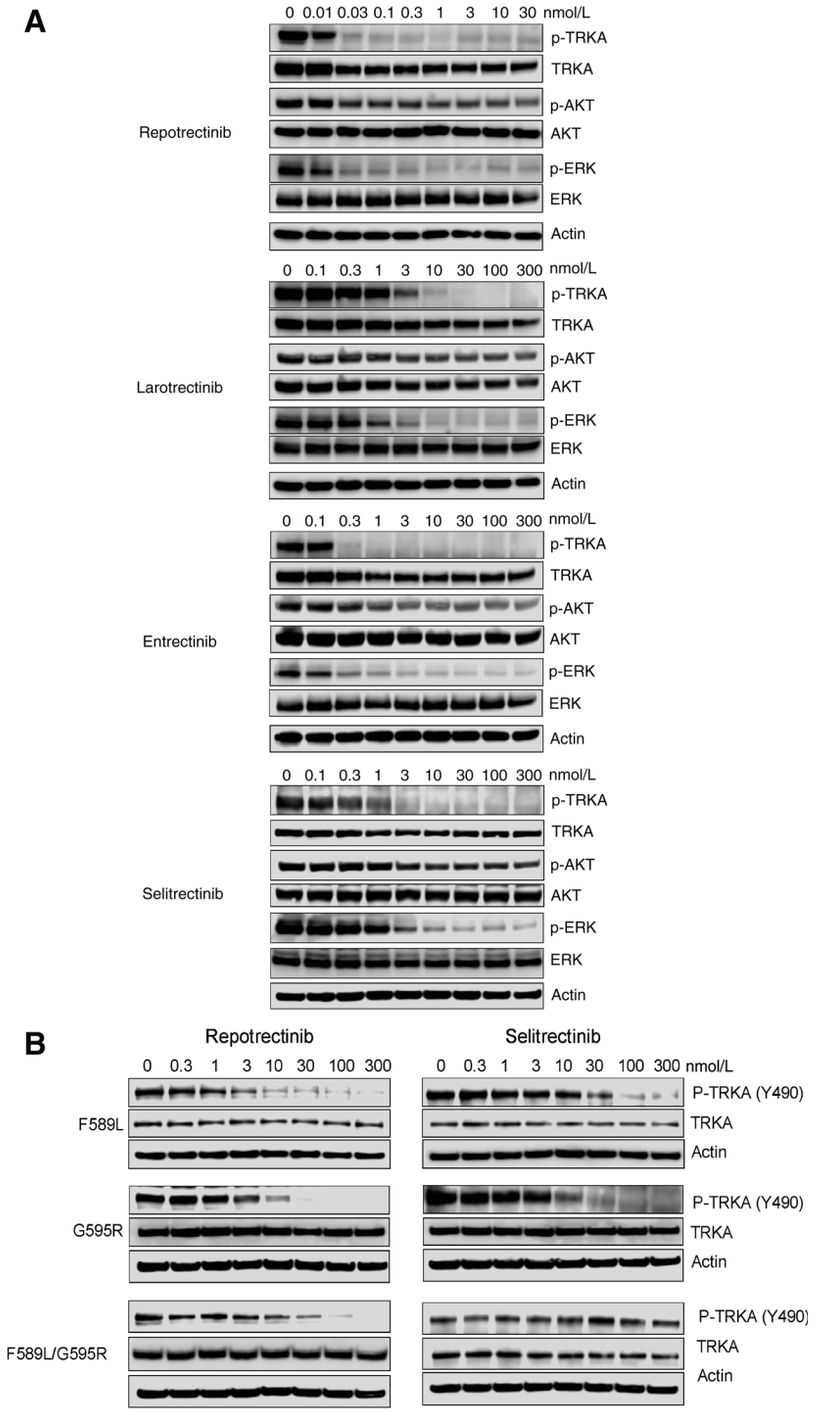

Figure 2.

Evaluation of inhibition of TRKA fusion protein autophosphorylation by larotrectinib, entrectinib, repotrectinib, and selitrectinib. **A,** KM12 cells (TPM3–TRKA) were treated with compounds for 4 hours and probed for TRKA phosphorylated on Tyr490 and for total TRKA. Because of the high potency of repotrectinib, a lower range of concentrations (0–30 nmol/L) was used relative to the other TRK inhibitors (0–300 nmol/L). **B,** Cellular evaluation of macrocyclic TRK inhibitors repotrectinib and selitrectinib against the gatekeeper mutation (F589L), the solvent-front mutation (G595R), and the gatekeeper/solvent-front (F589L/G595) compound mutant forms of *LMNA-TRKA* by evaluating TRKA autophosphorylation in NIH3T3-engineered cell lines.

(Supplementary Fig. S2A). The cocrystal structure of wild-type TRKA with repotrectinib shows that it adopts a DFG_{in} active conformation (**Fig. 3A**). The fluorophenyl group of repotrectinib makes a Dunitz interaction (20) with the amide carbonyl of Asn655 and the pyrazolopyrimidine heterocycle interacts closely with the hinge, accepting and donating hydrogen bonds with residues Glu590 and Met592, respectively (**Fig. 3B**). The cocrystal structure of repotrectinib with TRKA harboring a G595R SFM shows that it also adopts a DFG_{in} active conformation (**Fig. 3C**) and has complete electron density of repotrectinib bound in the active site of TRKA harboring the G595R mutation (Supplementary Fig. S2B). Critical to repotrectinib's potent inhibition of TRKA harboring the SFM G595R, the macrocycle does not interfere with the mutated Arg595 residue, which is observed to collapse over the binding pocket making a hydrogen bond to the carbonyl of Leu516 (**Fig. 3D**). The Arg595 position observed in the TRKA crystal structure is in contrast with modeling studies that predict it extends into

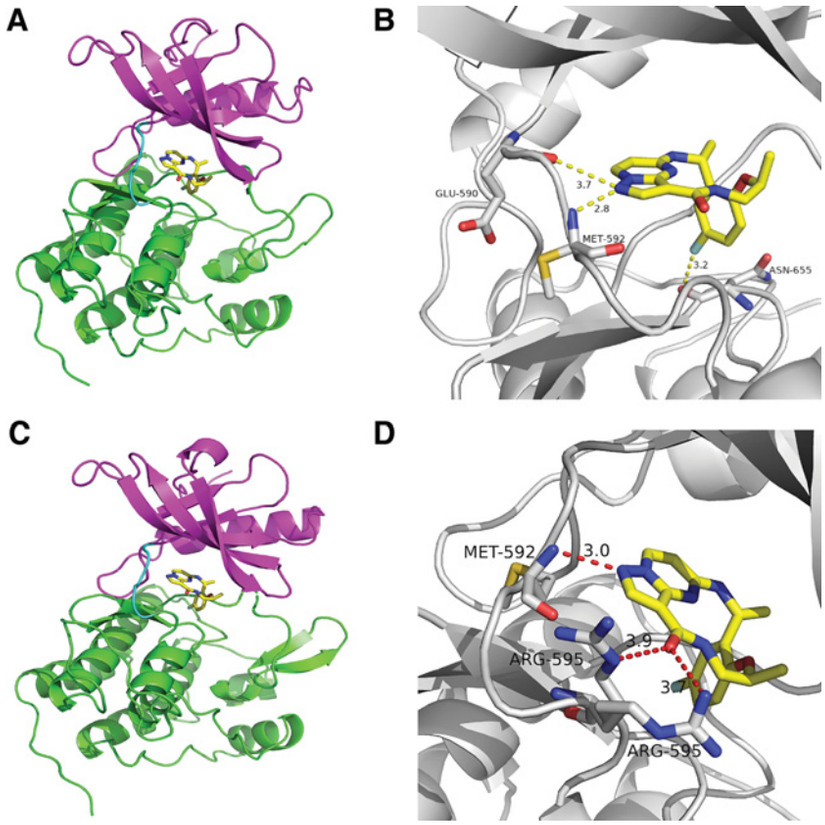

Figure 3.

Cocrystal structures of TRKA and TRKA^{G595R} with repotrectinib. **A,** Repotrectinib binds in the hinge region of the wild-type TRKA active site (N-lobe: magenta; C-lobe: green; hinge: cyan). **B,** Cocrystal structure of wild-type TRKA with repotrectinib (2.90 Å). Key protein–ligand interactions with the hinge are shown using red dashed lines (atom–atom distances in Å). **C,** Repotrectinib binding in the active site of TRKA^{G595R} (2.70 Å). **D,** Repotrectinib binds in the hinge region of the TRKA^{G595R} active site. Key protein–ligand interactions with hinge and the G595R sidechain are shown using red dashed lines (atom–atom distances in Å).

solvent (9, 14). An overlay of the bound structure of repotrectinib in wild-type TRKA and TRKA harboring the G595R mutation shows near-identical conformations (Supplementary Fig. S2C). The X-ray crystal structure of unbound repotrectinib was solved (Supplementary Fig. S2D; Supplementary Table S2) and compared with the conformation of repotrectinib bound to TRKA^{G595R}, which shows that the unbound conformation of repotrectinib is very similar to the bound conformation (Supplementary Fig. S2E). A conformational analysis of repotrectinib using *ab initio* calculations identifies only two low-energy conformations with one of them matching the conformation found in the cocrystal structures indicating there is a minimal energetic penalty upon binding to TRKA (Supplementary Fig. S2F; Supplementary Table S3). Repotrectinib has a conformationally restricted ethyl ether linker, which contributes to its conformational rigidity. A similar conformational analysis performed on selitrectinib shows that there are five low-energy conformations available to it derived from the piperidine ring and propyl linker regions of the macrocyclic structure (Supplementary Fig. S2F; Supplementary Table S3). Selitrectinib's methyl group is predicted to extend from the macrocycle in the direction of the Arg595 residue, suggesting a basis for reduced activity against this SFM. Similarly, GKM F589L, with its greater bulk, may interfere with the extended pyrrolidine ring of selitrectinib. Taken together, both steric and dynamic aspects of compact macrocycle structures contribute to the delivery of potent inhibition of wild-type and mutant TRK proteins.

Evaluation of inhibitors in tumor models of oncogenic TRK and drug-resistant TRK

For TRK inhibitors with cell potency against TRKA (wild-type, mutant), head-to-head comparisons were performed in *in vivo* xenograft tumor models. Previous efficacy studies of repotrectinib in two NIH3T3 engineered models of LMNA–TRKA and LMNA–TRKA^{G595R} included only high-dose entrectinib as comparator and did not include pharmacokinetic/pharmacodynamic analysis (14). The current study was designed to have drug exposures that are clinically achievable as well as including direct comparisons with both generations of TRK inhibitors. Repotrectinib drug exposure was shown to correlate with the degree of suppression of TRK fusion protein autophosphorylation at Tyr490 in a NIH3T3 LMNA–TRKA xenograft model (Supplementary Fig. S3A). Repotrectinib dosed at 3 mg/kg treatment resulted in incomplete suppression of TRKA autophosphorylation (85% and 56% inhibition at 3 hours and 12 hours, respectively) relative to 15 mg/kg repotrectinib (96% and 74% inhibition at 3 hours and 12 hours, respectively) and the degree of TRKA autophosphorylation suppression correlated with previously reported efficacy in this model (14). In addition, the PK/PD analysis (Supplementary Fig. S3A) shows that doses used in the xenograft tumor models have repotrectinib exposures that are clinically achievable based on previously reported repotrectinib human PK data (e.g., 160 mg dose, single patient 12 hours exposure: 560 nmol/L total, 26 nmol/L unbound concentration; ref. 14). A nonengineered model (KM12 tumor cell line, wild-type TPM3-TRKA) was used to test whether efficacy observed in engineered models (LMNA–TRKA NIH3T3 model, 15 mg/kg b.i.d. repotrectinib, 23% tumor regression; ref. 14) translated to a model of tumor cells. Treatment of the wild-type TPM3–TRKA KM12 xenograft model with 15 mg/kg b.i.d. repotrectinib resulted in 13% tumor regression, which is consistent with the results from the related engineered model (Supplementary Fig. S3B). Efficacy was evaluated in four engineered models harboring LMNA–TRKA^{G595R}, LMNA–TRKA^{F589L}, LMNA–TRKA^{G667C}, and LMNA–TRKA$^{F589L/G595R}$ (**Fig. 4**). In the LMNA–TRKA^{G595R}

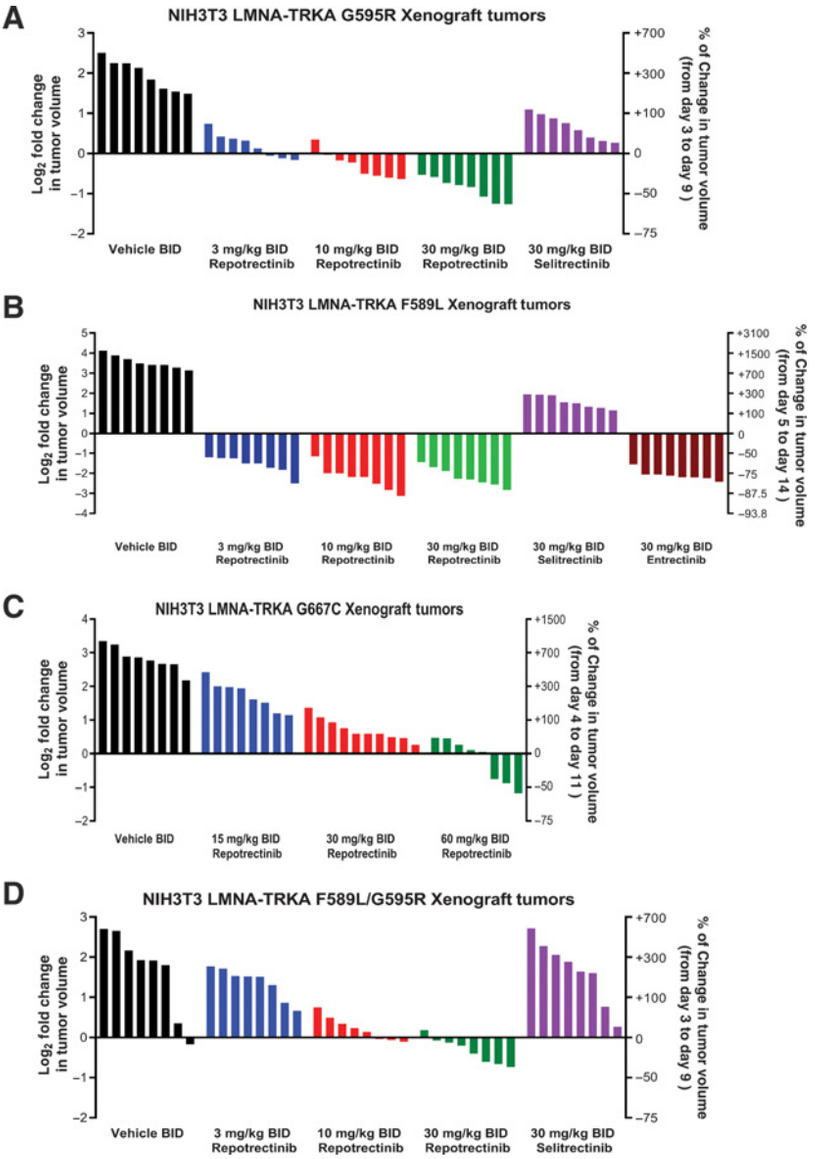

Figure 4.

Evaluation of TRK inhibitors against mutant TRKA-dependent xenograft tumor models. The plots show individual responses to the indicated treatments. **A,** Efficacy of repotrectinib and selitrectinib in NIH3T3 cell–derived xenograft model with LMNA–TRKA fusion harboring G595R solvent-front mutation. **B,** Antitumor effect of repotrectinib, entrectinib, and selitrectinib in NIH3T3 cell–derived xenograft model with LMNA–TRKA fusion harboring F589 L gatekeeper mutation. **C,** Evaluation of repotrectinib (15, 30, and 60 mg/kg b.i.d.) in an NIH3T3 *LMNA–TRKA*^{G667C} xenograft tumor model. **D,** Antitumor effect of repotrectinib and selitrectinib in the NIH3T3 cell–derived xenograft model with *LMNA–TRKA* fusion harboring an F589L/G595R compound mutation.

NIH3T3 xenograft model, repotrectinib at 3 mg/kg b.i.d., 10 mg/kg b.i.d., and 30 mg/kg b.i.d. dose levels resulted in 95% TGI, 19% tumor regression, and 46% tumor regression, respectively, whereas 30 mg/kg selitrectinib resulted in 80% TGI (**Fig. 4A**; Supplementary Fig. S4A). In the LMNA–TRKA^{F589L} NIH3T3–engineered xenograft model, repotrectinib was highly efficacious at low doses (3 mg/kg b.i.d., 67% tumor regression; 10 mg/kg b.i.d., 79% tumor regression; 30 mg/kg b.i.d., 78% tumor regression), whereas 30 mg/kg b.i.d. entrectinib dosing resulted in 77% tumor regression and 30 mg/kg b.i.d. selitrectinib dosing (dose selected based on published studies; ref. 9) resulted in 80% TGI (**Fig. 4B**; Supplementary Fig. S4B). The *in vivo* efficacy observed in the TRKA GKM tumor model for both repotrectinib and entrectinib is consistent with cellular results (**Table 1**). Because repotrectinib was the only TRK inhibitor that had potent inhibition of xDFG cell models (**Table 1**), it was the only inhibitor evaluated in an xDFG xenograft model. In the LMNA–TRKA^{G667C} NIH3T3 xenograft model of a xDFG mutation, repotrectinib had dose-dependent efficacies (15 mg/kg b.i.d., 60% TGI; 30 mg/kg b.i.d., 88% TGI; 60 mg/kg b.i.d., 7% tumor regression; **Fig. 4C**; Supplementary Fig. S4C). In the LMNA–TRKA$^{F589L/G595R}$ NIH3T3 xenograft model, repotrectinib dosed at 10 mg/kg b.i.d. and 30 mg/kg b.i.d. led to 93% TGI and 16% tumor regression, respectively, whereas 30 mg/kg b.i.d. selitrectinib dosing did not produce statistically significant TGI (**Fig. 4D**; Supplementary Fig. S4D). Body-weight gain was observed in the LMNA–TRKA^{F589L} tumor model for mice in the vehicle treatment group and animals in all of the treatment arms (Supplementary Fig. S5A) as well as for repotrectinib treated mice in the LMNA–TRKA^{G667C} NIH3T3 xenograft model (Supplementary Fig. S5B). These findings suggest that repotrectinib is highly efficacious in wild-type, single-mutant, and compound mutation TRKA-dependent xenograft tumor models, with results that are well correlated with cell potency.

Clinical activity of repotrectinib

TRIDENT-1 (NCT03093116) is a global, open-label phase II study of repotrectinib currently being conducted in up to 120 centers with a targeted enrollment of approximately 320 patients in six defined

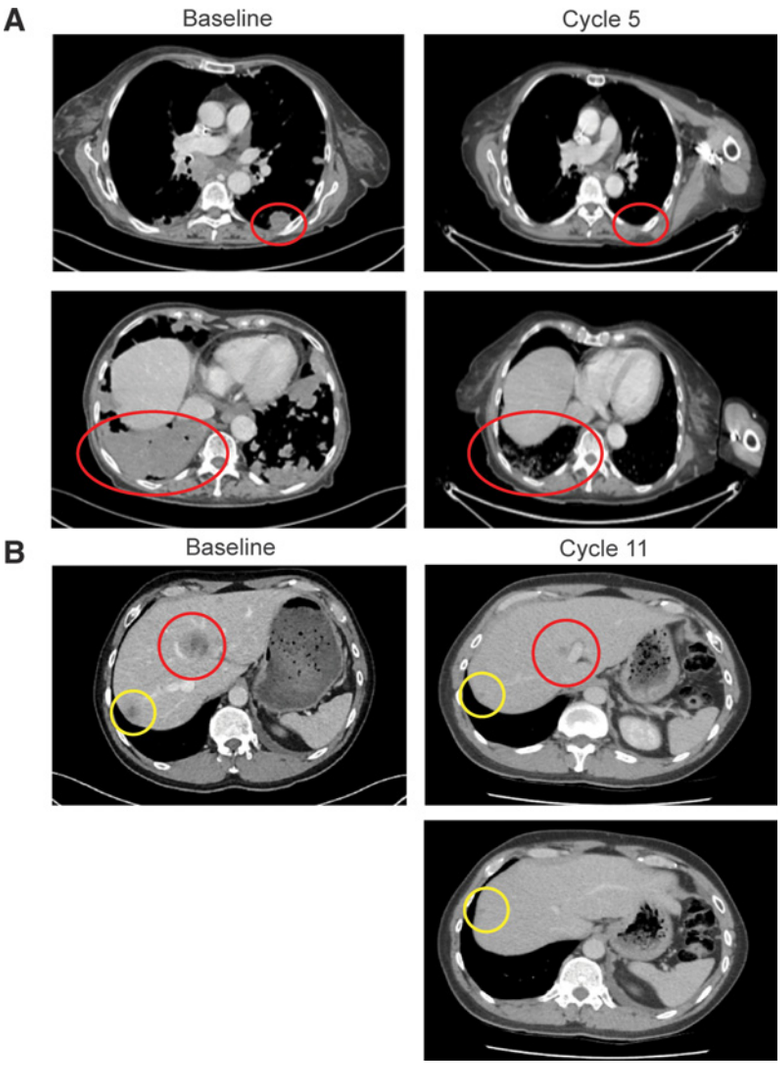

Figure 5.
Clinical proof-of-concept cases of the repotrectinib activity in TKI-naïve and TKI-pretreated patients with *NTRK* fusion–positive cancers. **A,** A treatment-naïve 79-year-old female with *NTRK3* rearranged metastatic NSCLC was diagnosed in July 2020. The patient enrolled in the TRIDENT-1 trial in July of 2020, achieved 54% tumor regression by investigator assessment after 6 months of treatment, and as of April 23, 2021, remained on treatment with duration of response of 3.7+ months and duration of treatment of 7.2+ months. **B,** A 43-year-old male with *EML4–NTRK3* metastatic NSCLC who progressed on entrectinib treatment with a G623R solvent-front mutation enrolled in the TRIDENT-1 trial on December 12, 2019, demonstrated 65% tumor regression after 10 months of treatment, and was still on treatment as of April 23, 2021.

expansion (EXP) cohorts: *ROS1*$^+$ advanced NSCLC (EXP-1–EXP-4) and *NTRK*$^+$ advanced solid tumors (EXP-5 and EXP-6). Clinical proof-of-concept cases of the activity of repotrectinib in TKI-naïve and TKI-pretreated patients with *NTRK* fusion–positive cancers were selected from the ongoing TRIDENT-1 study. A treatment-naïve 79-year-old female with *NTRK3*-rearranged metastatic NSCLC diagnosed in July 2020 was enrolled into EXP-5 (*NTRK*$^+$ TKI-naïve advanced solid tumors). The patient achieved 32% tumor regression by investigator assessment after 2 months of repotrectinib treatment and 54% tumor regression after 6 months of treatment (**Fig. 5A**). As of April 23, 2021, patient remained on treatment with duration of response of 3.7+ months and duration of treatment of 7.2+ months. A 45-year-old male with metastatic NSCLC initially diagnosed in September 2018 was enrolled into EXP-6 (*NTRK*$^+$ TKI-pretreated advanced solid tumors) of the TRIDENT-1 phase II study. The patient's medical history included initial treatment with carboplatin/paclitaxel chemotherapy. An *EML4–NTRK3* rearrangement was detected in November 2018, and the patient was treated with entrectinib for 12 months with a partial response. The patient progressed on entrectinib with emergence of a G623R solvent-front resistance mutation (no brain metastases) and was subsequently enrolled into the repotrectinib TRIDENT-1 study in December 2019. The patient achieved 50% tumor regression by investigator assessment after 4 months of repotrectinib treatment and 65% tumor regression after 10 months of treatment (**Fig. 5B**). As of 23 April 2021, the patient remained on treatment with duration of response of 9.2+ months and duration of treatment of 16.4+ months. These interim data from the TRIDENT-1 study demonstrate the clinical activity of repotrectinib in patients with TKI-naïve and TKI-pretreated *NTRK*+ cancers.

Discussion

The durability of clinical response to first-generation kinase-targeted therapies is often limited by mutations that affect inhibitor binding interactions. To overcome resistance mutations, patients are often treated with a second targeted therapy that has a different mutant susceptibility profile. However, with each subsequent treatment, the disease can become more complex and harder to treat (21). First-line therapies that are highly potent against the wild-type oncogenic kinase via binding interactions that avoid mutational hotspots have been reported to have enhanced clinical benefit. The third-generation EGFR inhibitor osimertinib, which inhibits both oncogenic driver mutations

(e.g., L858R, exon 19 deletions) and the primary resistance mutation (T790M), was reported to deliver significantly longer overall survival relative to earlier generation inhibitors (22) and third-generation ALK inhibitor lorlatinib treatment of NSCLC patients resulted in longer progression-free survival relative to the first-generation inhibitor crizotinib (23). Molecular attributes of the compact macrocycle architecture may be ideal to potently inhibit wild-type oncogenic kinases while being less susceptible to resistant mutations because of their small binding interface (4, 9, 14). However, specific molecular attributes of a compact macrocycle are critical to biological performance. The current study shows that the second-generation TRK inhibitors have significantly different potencies against both wild-type and mutant forms of TRK, with repotrectinib being at least 10-fold more potent than selitrectinib in wild-type and mutant TRKA/B/C cellular assays. In the case of GKMs, repotrectinib was 140–430-fold more potent than selitrectinib, whereas differences were more variable for SFMs, with 11- to 95-fold differences. Absolute potency of an inhibitor may be important because it can contribute to overall *in vivo* efficacy through time-dependent target engagement in an environment where both drug and target concentrations vary as a function of time (24–26). Interestingly, the TRK protein context (e.g., TRKA vs. TRKB vs. TRKC) was found to have little effect on inhibitor potency with the exception of the GKMs. As the gatekeeper residue is part of a "hydrophobic shell" that regulates intramolecular communication through interactions with both hydrophobic spines (27), TRK isoform–specific effects are reasonable because the conformational dynamics of each TRK isoform may be distinct. Taken together, specific molecular characteristics of repotrectinib's compact macrocyclic structure enable it to potently inhibit wild-type TRK fusion proteins as well as TRK-harboring mutations that cause resistance to previous generations of TRK inhibitors.

Understanding the molecular underpinnings of the TRK potency profiles of repotrectinib and selitrectinib requires structural analyses. To date, there has been a dearth of cocrystal structures of compact macrocyclic kinase inhibitors, limiting both our understanding of binding interactions and the precision of molecular modeling analyses. In the current study, repotrectinib cocrystal structures with TRKA illuminate specific interactions, or lack of interactions, with TRKA and mutant TRKA that enable potent inhibition. These studies show that repotrectinib does not extend into the solvent-front or gatekeeper regions, whereas the modeled structure of selitrectinib has the potential for adverse steric interactions. Structural and energetic analyses revealed that repotrectinib adopts a solution state conformation that is nearly identical to the bound conformation for both wild-type and $TRKA^{G595R}$, which is expected to contribute to its high potency with a small binding interface from reduced entropic penalties to binding (Supplementary Fig. S2). Molecular modeling studies of repotrectinib and selitrectinib show that repotrectinib has a more conformationally constrained macrocyclic structure, which is likely to contribute to its greater potency relative to selitrectinib. Molecular modeling of selitrectinib bound to TRK based on the repotrectinib/TRKA cocrystal structures predict that selitrectinib extends into the gatekeeper region, which is well correlated with the larger loss of potency relative to other mutations. Both steric and conformational aspects of the macrocyclic structure of repotrectinib are therefore consistent with its cellular and *in vivo* performance, specifically its potent inhibition of wild-type and mutant TRKs, relative to other tested TRK inhibitors.

In the course of the structural analysis, an unexpected interaction was observed in the $TRKA^{G595R}$ cocrystal structures—the G595R guanidine sidechain does not extend out to solvent as previous modeling studies have predicted (9, 14) but folds back into the active site, forming a stable interaction with the protein backbone (**Fig. 3D**). This unusual intramolecular arrangement forms a stabilized structure that is bulky and likely hard to displace. Previous modeling studies on a related tyrosine kinase (ALK) hypothesized that there is a similar intramolecular interaction, although it was not supported by crystallographic evidence (24). Interestingly, the G/R drug-resistance mutation is commonly found in patients with TRK fusions and other RTKs (e.g., ALK, RET, and ROS1; refs. 28–30), but its prevalence cannot be explained by codon probabilities. The G/R mutation is a radical point mutation (small, flexible hydrogen sidechain mutated to a large, charged guanidino group) and a recent analysis of the codon code shows that it is biased to maintain protein structure by favoring conservative amino acid changes for single-nucleotide substitutions (e.g., aliphatic for aliphatic mutations; ref. 31). Further, mutations of glycine and proline have the highest probability for self-preservation (i.e., nucleotide changes resulting in no amino acid change). As such, G/R mutations are possible, albeit with a low probability, and the frequent occurrence of G/R SFMs as a resistance mechanism is likely due to evolutionary selection based on the unique sidechain intramolecular interactions.

Compound mutations in the kinase domain have been found in patients treated with many types of kinase-targeted therapies (e.g., ABL, ALK, RET, and ROS1 inhibitors; refs. 11–13) and may occur in patients treated with TRK inhibitors. Resistance arising as a result of compound mutations can be challenging because these mutations create multiple alterations to the kinase active site and it has been difficult to anticipate drug efficacy. Compact macrocyclic inhibitors have the potential to address resistance from compound mutations because their small, efficient binding interface can fit entirely inside the active-site cleft. However, their specific binding interactions are critical to whether the inhibitor is effective. The combination of a small binding interface and an optimal unbound conformation enables repotrectinib to potently inhibit TRKA harboring a compound mutation. In the case of selitrectinib, the combination of adverse steric interactions with individual mutations (e.g., GKM) and conformational flexibility hinder selitrectinib from achieving potent inhibition toward the compound mutations tested in the current study. Therefore, specific attributes of the repotrectinib macrocyclic structure make it the only TRK inhibitor tested to date that potently inhibits TRKA harboring a compound mutation.

Finally, this study presents additional clinical proof-of-concept data of the activity of repotrectinib in patients, consistent with its Fast Track designation for patients with $NTRK^{+}$ advanced solid tumors previously treated with chemotherapy and TRK TKI and no alternative treatments. The potency of repotrectinib against wild-type TRK fusions and broad activity against single mutations supports its potential use in TKI-naïve patients with *NTRK* fusion–positive cancers as a means of delaying or preventing on-target resistance. This strategy of using a TKI as first-line therapy that is effective against both the primary target as well as resistance variants would be similar to the use of osimertinib and alectinib in TKI-naïve EGFR-mutant and ALK^{+} lung cancers, respectively. The TRIDENT-1 trial continues to explore the activity of repotrectinib in patients with TKI-naïve and TKI-pretreated $NTRK^{+}$ advanced solid tumors, in addition to patients with $ROS1^{+}$ NSCLC for which Breakthrough Therapy and Fast Track designations have been granted.

In conclusion, the current study utilizes a wide array of experimental approaches to understand the precise molecular characteristics of compact macrocyclic inhibitor structure that enable potent inhibition of oncogenic TRK fusion proteins as well as reduce the susceptibility to drug resistance. From this work, subtle but important aspects of

compact macrocycle structure are defined that should serve as a foundation for the design of inhibitors that target other oncogenic kinases.

Authors' Disclosures

B.W. Murray reports other support from Turning Point Therapeutics outside the submitted work. P.A. Sprengeler reports other support from Turning Point Therapeutics during the conduct of the study. S.H. Reich reports personal fees from Turning Point Therapeutics Inc. outside the submitted work. S. Stopatschinskaja reports other support from Turning Point Therapeutics during the conduct of the study and is employed by Turning Point Therapeutics. B. Solomon reports other support from Turning Point Therapeutics during the conduct of the study. B. Besse reports grants from 4D Pharma, AbbVie, Amgen, Aptitude Health, AstraZeneca, BeiGene, Blueprint Medicines, BMS, Boehringer Ingelheim, Celgene, Cergentis, Cristal Therapeutics, Daiichi-Sankyo, Eli Lilly, GSK, Inivata, Janssen, Onxeo, OSE Immunotherapeutics, Pfizer, Roche-Genentech, Sanofi, Takeda, and Tolero Pharmaceuticals during the conduct of the study. A. Drilon reports personal fees from TP Therapeutics during the conduct of the study; personal fees from Nuvalent, Ignyta/Genentech/Roche, Loxo/Bayer/Lilly, Takeda/Ariad/Millenium, AstraZeneca, Pfizer, Blueprint Medicines, Helsinn, Beigene, BergenBio, Hengrui Therapeutics, Exelixis, Tyra Biosciences, Verastem, MORE Health, AbbVie, 14ner/Elevation Oncology, Remedica Ltd., ArcherDX, Monopteros, Novartis, EMD Serono, Melendi, Liberum, Repare RX, Chugai, and Merus outside the submitted work; and associated research paid to institution: Pfizer, Exelixis, GlaxoSmithKlein, Teva, Taiho, PharmaMar; royalties: Wolters Kluwer; other (food/beverage): Merck, Puma, Merus, Boehringer Ingelheim; CME Honoraria: Medscape, OncLive, PeerVoice, Physicians Education Resources, Targeted Oncology, Research to Practice, Axis, Peerview Institute, Paradigm Medical Communications, WebMD, MJH Life Sciences, AXIS, EPG Health, JNCC/Harborside. No disclosures were reported by the other authors.

Authors' Contributions

B.W. Murray: Conceptualization, data curation, formal analysis, supervision, validation, writing–original draft, writing–review and editing. **E. Rogers:** Conceptualization, data curation, formal analysis, supervision, visualization, methodology, writing–review and editing. **D. Zhai:** Resources, data curation, formal analysis, supervision, methodology, writing–original draft, writing–review and editing. **W. Deng:** Resources, data curation, formal analysis, supervision, validation, writing–original draft, writing–review and editing. **X. Chen:** Formal analysis, visualization, methodology, writing–original draft, writing–review and editing. **P.A. Sprengeler:** Data curation, formal analysis, methodology, writing–original draft, writing–review and editing. **X. Zhang:** Data curation, formal analysis, methodology. **A. Graber:** Writing–review and editing. **S.H. Reich:** Writing–review and editing. **S. Stopatschinskaja:** Writing–original draft, writing–review and editing. **B. Solomon:** Writing–review and editing. **B. Besse:** Writing–review and editing. **A. Drilon:** Writing–original draft, writing–review and editing.

Acknowledgments

All work was funded by Turning Point Therapeutics.

The costs of publication of this article were defrayed in part by the payment of page charges. This article must therefore be hereby marked *advertisement* in accordance with 18 U.S.C. Section 1734 solely to indicate this fact.

Received July 20, 2021; revised July 28, 2021; accepted October 1, 2021; published first October 8, 2021.

References

1. Drilon A. TRK inhibitors in TRK fusion-positive cancers. Ann Oncol 2019;30: viii23–30.
2. Cocco E, Scaltriti M, Drilon A. NTRK fusion-positive cancers and TRK inhibitor therapy. Nat Rev Clin Oncol 2018;15:731–47.
3. Amatu A, Sartore-Bianchi A, Bencardino K, Pizzutilo EG, Tosi F, Siena S. Tropomyosin receptor kinase (TRK) biology and the role of NTRK gene fusions in cancer. Ann Oncol 2019;30:viii5–viii153.
4. Laetsch TW, Hong DS. Tropomyosin receptor kinase inhibitors for the treatment of TRK fusion cancer. Clin Cancer Res 2021;27:4974–82.
5. Hong DS, DuBois SG, Kummar S, Farago AF, Albert CM, Rohrberg KS, et al. Larotrectinib in patients with TRK fusion-positive solid tumours: a pooled analysis of three phase 1/2 clinical trials. Lancet Oncol 2020;21: 531–40.
6. Doebele RC, Drilon A, Paz-Ares L, Siena S, Shaw AT, Farago AF, et al. Entrectinib in patients with advanced or metastatic NTRK fusion-positive solid tumours: integrated analysis of three phase 1–2 trials. Lancet Oncol 2020;21:271–82.
7. Drilon A, Laetsch TW, Kummar S, DuBois SG, Lassen UN, Demetri GD, et al. Efficacy of larotrectinib in TRK fusion-positive cancers in adults and children. N Engl J Med 2018;378:731–9.
8. Drilon A, Li G, Dogan S, Gounder M, Shen R, Arcila M, et al. What hides behind the MASC: clinical response and acquired resistance to entrectinib after ETV6-NTRK3 identification in a mammary analogue secretory carcinoma (MASC). Ann Oncol 2016;27:920–62.
9. Drilon A, Nagasubramanian R, Blake JF, Ku N, Tuch BB, Ebata K, et al. A next-generation TRK kinase inhibitor overcomes acquired resistance to prior TRKkinase inhibition in patients with TRK fusion-positive solid tumors. Cancer Discov 2017;7:963–72.
10. Russo M, Misale S, Wei G, Siravegna G, Crisafulli G, Lazzari L, et al. Acquired resistance to the TRK inhibitor entrectinib in colorectal cancer. Cancer Discov 2016;6:36–44.
11. Zabriskie MS, Eide CA, Tantravahi SK, Vellore NA, Estrada J, Nicolini FE, et al. BCR-ABL1 compound mutations combining key kinase domain positions confer clinical resistance to ponatinib in Ph chromosome-positive leukemia. Cancer Cell 2014;26:428–42.
12. Yoda S, Lin JJ, Lawrence MS, Burke BJ, Friboulet L, Langenbucher A, et al. Sequential ALK inhibitors can select for lorlatinib-resistant compound ALK mutations in ALK-positive lung cancer. Cancer Discov 2018;8:714–29.
13. Khorashad JS, Kelley TW, Szankasi P, Mason CC, Soverini S, Adrian LT, et al. BCR-ABL1 compound mutations in tyrosine kinase inhibitor-resistant CML: frequency and clonal relationships. Blood 2013;121:489–98.
14. Drilon A, Ou SI, Cho BC, Kim DW, Lee J, Lin JJ, et al. Repotrectinib (TPX-0005) Is a next-generation ROS1/TRK/ALK inhibitor that potently inhibits ROS1/TRK/ALK solvent-front mutations. Cancer Discov 2018;8:1227–36.
15. Poulsen AU, Dymock BW. Small molecule macrocyclic kinase inhibitors. In: Ward RA, Goldberg FW, editors. Kinase drug discovery: modern approaches. Volume 67, Drug Discovery Series. London, UK: Royal Society of Chemistry; 2019:97–127.
16. Cho BC, Drilon AE, Doebele RC, Kim D-W, Lin JJ, Lee J, et al. Safety and preliminary clinical activity of repotrectinib in patients with advanced ROS1 fusion-positive non-small cell lung cancer (TRIDENT-1 study). J Clin Oncol 37: 15s, 2019 (suppl. abstr. 9011).
17. Lanman RB, Mortimer SA, Zill OA, Sebisanovic D, Lopez R, Blau S, et al. Analytical and clinical validation of a digital sequencing panel for quantitative, highly accurate evaluation of cell-free circulating tumor DNA. PLoS One 2015; 10:e0140712.
18. Biarc J, Chalkley RJ, Burlingame AL, Bradshaw RA. Dissecting the roles of tyrosines 490 and 785 of TrkA protein in the induction of downstream protein phosphorylation using chimeric receptors. J Biol Chem 2013;288: 16606–18.
19. Obermeier A, Bradshaw RA, Seedorf K, Choidas A, Schlessinger J, Ullrich A. Neuronal differentiation signals are controlled by nerve growth factor receptor/Trk binding sites for SHC and PLC gamma. EMBO J 1994;13:1585–90.
20. Burgi HB, Dunitz JD, Shefter E. Geometrical reaction coordinates. II. Nucleophilic addition to a carbonyl group. J Am Chem Soc 1973;95:5065–7.
21. Bozic I, Nowak M. Resisting resistance. Annual Review of Cancer Biology 2017;1: 203–21.
22. Ramalingam SS, Vansteenkiste J, Planchard D, Cho BC, Gray JE, Ohe Y, et al. Overall survival with osimertinib in untreated, EGFR-mutated advanced NSCLC. N Engl J Med 2020;382:41–50.
23. Shaw AT, Bauer TM, de Marinis F, Felip E, Goto Y, Liu G, et al. First-line lorlatinib or crizotinib in advanced ALK-positive lung cancer. N Engl J Med 2020;383:2018–29.
24. Chuang YC, Huang BY, Chang HW, Yang CN. Molecular Modeling of ALK L1198F and/or G1202R mutations to determine differential crizotinib sensitivity. Sci Rep 2019;9:11390.

25. Peters SA, Petersson C, Blaukat A, Halle JP, Dolgos H. Prediction of active human dose: learnings from 20 years of Merck KGaA experience, illustrated by case studies. Drug Discov Today 2020;25:909–19.
26. Tonge PJ. Drug-target kinetics in drug discovery. ACS Chem Neurosci 2018;9: 29–39.
27. Taylor SS, Meharena HS, Kornev AP. Evolution of a dynamic molecular switch. IUBMB Life 2019;71:672–84.
28. Dagogo-Jack I, Rooney M, Lin JJ, Nagy RJ, Yeap BY, Hubbeling H, et al. Treatment with next-generation ALK inhibitors fuels plasma ALK mutation diversity. Clin Cancer Res 2019;25:6662–70.
29. Solomon BJ, Tan L, Lin JJ, Wong SQ, Hollizeck S, Ebata K, et al. RET solvent front mutations mediate acquired resistance to selective RET inhibition in RET-driven malignancies. J Thorac Oncol 2020;15:541–9.
30. Yun MR, Kim DH, Kim SY, Joo HS, Lee YW, Choi HM, et al. Repotrectinib exhibits potent antitumor activity in treatment-naive and solvent-front-mutant ROS1-rearranged non-small cell lung cancer. Clin Cancer Res 2020;26:3287–95.
31. Chan KF, Koukouravas S, Yeo JY, Koh DW, Gan SK. Probability of change in life: amino acid changes in single nucleotide substitutions. Biosystems 2020;193–194: 104135.